Microstructural effects on stress in thin films

Von der Fakultät Chemie der Universität Stuttgart
zur Erlangung der Würde eines Doktors der Naturwissenschaften (Dr. rer. nat.)
genehmigte Abhandlung

vorgelegt von

Markus Albin Wohlschlögel

aus Aschaffenburg

Hauptberichter:	Prof. Dr. Ir. E. J. Mittemeijer
Mitberichter:	Prof. Dr. F. Aldinger
Prüfungsvorsitzender:	Prof. Dr. E. Roduner
Tag der Einreichung:	23.06.2008
Tag der mündlichen Prüfung:	16.09.2008

MAX-PLANCK-INSTITUT FÜR METALLFORSCHUNG STUTTGART
INSTITUT FÜR METALLKUNDE DER UNIVERSITÄT STUTTGART

Stuttgart, 2008

Contents

1. General introduction 9

1.1. Global view and historical background..9

1.1.1. Technological relevance of thin films 9

1.1.2. Scientific relevance of thin film/layer systems 10

1.1.2.1. Thin film fabrication.. 10

1.1.2.2. Microstructure of thin films grown by deposition.. 11

1.1.2.3. Thin layers grown by gas nitriding of pure iron... 11

1.1.2.4. Properties of thin film/layer systems; effects related to a nanocrystalline microstructure.. 16

1.2. Focus of the thesis 20

1.3. Methodology and interpretation strategies.....................................20

1.4. Outline of the thesis...25

2. Unexpected formation of ε iron nitride by gas nitriding of nanocrystalline α-Fe films..29

2.1. Introduction 30

2.2. Experimental..30

2.3. Results and discussion...31

2.4. Conclusions 37

3. Crystallite-size dependence of the coefficient of thermal expansion of metals 39

3.1. Introduction 40

3.2. Experimental...41

3.3. Results and discussion..42

3.4. Conclusions 47

4. Determination of depth gradients of grain interaction and stress in Cu thin films 51

4.1. Introduction 52

4.2. Theoretical background 53

4.2.1. Diffraction measurements at fixed penetration depth 53

4.2.2. Refraction and surface-roughness effects...................................... 54

4.2.3. The $f(\psi, hkl)$-method; determination of effective grain interaction 55

4.3. Experimental..56

4.3.1. Specimen preparation 56

4.3.2. Focused ion beam microscopy 56

4.3.3. Surface topography... 57

4.3.4. X-ray diffraction measurements 57

4.4. Results and Discussion 59

4.4.1. Grain morphology and film thickness 59

4.4.2. Surface roughness.. 60

4.4.3. Crystallographic texture 60

4.4.4. Stresses and grain interaction as function of depth 62

4.5. Conclusions 68

5. Residual stress and strain-free lattice-parameter depth profiles in a γ'-Fe_4N_{1-x} layer on an α-Fe substrate measured by X-ray diffraction stress analysis at constant information depth 73

5.1. Introduction 74

5.2. Theoretical background 76

5.2.1. X-ray residual stress analysis (XRSA) 76

5.2.2. Grain-interaction models 77

5.2.3. Determination of real-space depth profiles from XRSA at constant penetration/information depth 78

5.3. Experimental......80
5.3.1. Specimen preparation......80
5.3.2. Metallography......80
5.3.3. X-ray diffractometry......81
5.4. Results and discussion......82
5.4.1. Microstructure and phase analysis......82
5.4.2. Diffraction analysis at constant penetration depth......84
5.4.2.1. Lattice-parameter and nitrogen-concentration depth profiles......85
5.4.2.2. Residual stress depth profile......90
5.5. Conclusions......91
6. Application of a single-reflection collimating multilayer optic for X-ray diffraction experiments employing parallel-beam geometry ..97
6.1. Introduction......99
6.2. Background......100
6.2.1. Geometry conventions......100
6.2.1.1. Frames of reference......100
6.2.1.2. Diffraction geometry......101
6.2.2. Instrumental aberrations in parallel-beam X-ray diffraction......102
6.2.2.1. Illuminated and detected areas......102
6.2.2.2. Defocusing......103
6.2.3. Functional principle of a single-reflection collimating X-ray mirror......103
6.2.3.1. Two dimensional beam shaping by mirror optics......104
6.2.3.2. Single-reflection mirrors......105
6.3. Ray-tracing simulations......106
6.4. Experimental......111
6.5. Experimental results and discussion......112
6.5.1. Beam divergence and beam shape......112
6.5.2. Primary beam intensity and brilliance......114

6.5.3. Instrumental effects in XRD experiments employing parallel-beam geometry 117
6.5.3.1. Peak shape 117
6.5.3.2. Peak intensity 119
6.6. Comparative discussion 120
6.6.1. Simulation versus experiment 120
6.6.2. X-ray mirrors versus X-ray lenses 120
6.7. Summary 123
7. Kurzfassung der Dissertation in deutscher Sprache 127
7.1. Einleitung 127
7.2. Unerwartete Bildung von ε-Eisennitrid beim Gasnitrieren nanokristalliner α-Fe-Schichten 127
7.3. Kristallitgrößenabhängigkeit des thermischen Ausdehnungskoeffizienten von Metallen 128
7.4. Bestimmung von Gradienten effektiver Kornwechselwirkung und Spannung in dünnen Cu-Schichten 130
7.5. Tiefenprofile von Eigenspannung und dehnungsfreiem Gitterparameter in einer γ'-Fe_4N_{1-x}-Schicht 133
7.6. Anwendung einer kollimierenden Einfachreflektions-Multilagenoptik für Röntgenbeugungsexperimente in Parallelstrahlgeometrie 135
8. Summary 137
8.1. Introduction 137
8.2. Unexpected formation of ε-iron nitride by gas nitriding of nanocrystalline α-Fe films 137

8.3. Crystallite-size dependence of the coefficient of thermal expansion of metals 138

8.4. Determination of gradients of effective grain interaction and stress in Cu thin films..140

8.5. Residual stress and strain-free lattice parameter depth profiles in a γ’-Fe_4N_{1-x}-layer..142

8.6. Application of a collimating single reflection multilayer optic for X-ray diffraction experiments in parallel-beam geometry..................144

1. General introduction

1.1. Global view and historical background

1.1.1. Technological relevance of thin films

Miniaturisation is one of the key issues of today's technology and thin films are a vital part of it. The rapid development of highly integrated electronic devices is a direct result of the substantial progress in thin film research which has lead to a spectrum of applications ranging from conductor paths to compound semiconductor epitaxial thin film structures.

Moreover, thin films are essential components of many micro-electro-mechanical systems, where they serve as sensors or actuators. For instance, piezoelectric or piezoresistive thin films deposited on a silicon membrane are employed to detect a deflection of this membrane as a result of a pressure change electronically. Such a device can be used as a microphone in hearing aids [1].

Other major fields of application of thin films are coatings for optical, decorative, environmental or wear resistant use. As application examples anti-reflective coatings for camera lenses and glasses, metallic coatings for the creation of shiny surfaces, thermal barrier coatings in gas turbine engines and titanium nitride wear-protective coatings for tools are mentioned here.

Thin film technology is, however, not employed as recently as in the industrialised age: Already in ancient Egypt thin film coatings made of hammered gold were used for ornamentation and protection purposes: Gold leaf coatings from Luxor dating to the 18th dynasty (1567 – 1320 B.C.) exhibited thicknesses in the range of a few 100 nm's [2].

1.1.2. Scientific relevance of thin film/layer systems

Many actual applications of thin film systems are the result of fundamental research activities dealing with their fabrication as well as their interesting properties which can significantly differ from those of bulk materials.

1.1.2.1. Thin film fabrication

Two major thin film fabrication procedures are physical vapour deposition (PVD) and chemical vapour deposition (CVD). Whereas PVD-processes rely on the transfer of condensed matter into the gas phase by physical mechanisms as evaporation or sputtering, CVD-processes are characterized by the chemical reaction of a volatile compound of a material to be deposited with other compounds in the gas phase to produce a non-volatile solid which then deposits on a suitably placed substrate [3]. The earliest experiments on PVD-processes date back to the 19th century: In 1852 Grove found metal deposits which were sputtered from a cathode as a result of a glow discharge plasma [4] and in 1857 Faraday evaporated thin films while he was experimenting with exploding metal wires in an inert atmosphere [5]. Because of the fact that CVD-processes do not require vacuum or exceptional amounts of electric power they were commercially employed earlier than PVD-processes. Thus, already at the end of the 19th century CVD-processes were employed to deposit protective refractory metal coatings onto carbon wires which were used as illuminants in electric lamps at that time [6]. For more details on thin film deposition techniques the reader is referred to the book of Ohring [3].

Apart from deposition (i.e. creating a thin film structure on a usually much thicker substrate) thin layers on thick substrates can also be generated by reactions and phase transformations at surfaces. As an example the reaction of iron with nitrogen to form iron nitrides is mentioned here, as it plays an important role in this work. In this context nitrogen is provided by a mixture of ammonia and hydrogen in the gas phase which is referred to as gas- or gaseous nitriding [7]. One major difference to thin film deposition techniques is that in the case of nitriding the thin layer grows *into* the substrate, whereas the result of a PVD- or CVD-process is a thin film structure grown *onto* a substrate.

1.1.2.2. Microstructure of thin films grown by deposition

The microstructure of thin films deposited onto a substrate as well as that of thin layers grown into a substrate has been studied extensively as its features affect the mechanical behaviour of the films and the layers, respectively.

For deposited thin films the results of these works are structure-zone models describing the film microstructure as function of various deposition parameters. For the case of deposited thin films the scope will be limited to the PVD-processes sputtering and evaporation as they constitute the deposition techniques employed in this work. The earliest structure-zone model has been devised by Movchan and Demchishin in 1969 based on experimental investigations on thick evaporated metal and oxide coatings with various thicknesses [8]. Eight years later Thornton proposed a four-zone model describing the microstructure of sputtered thin films as a function of working gas pressure and substrate temperature [9]. More sophisticated structure-zone models have been developed since then conducting a systematic study of several evaporated elemental films with constant thickness [10] and taking into account the effect of ion bombardment in sputtered thin films [11].

1.1.2.3. Thin layers grown by gas nitriding of pure iron

Due its technological importance as hardening mechanism for steel, gas nitriding and the microstructure of nitrided iron have also been investigated extensively (see, for example Refs. [7,12,13] and references therein). Depending on nitriding temperature and composition of the nitriding gas atmosphere, and thus the activity of nitrogen in the gas phase, quantified by the nitriding potential (for details see below and, for example, [12]), compound layers composed of different phases can develop and/or nitrogen can react with iron forming iron nitride precipitates and can be interstitially dissolved in the iron matrix building a diffusion zone (see Figure 1.1). The compound layer is characterised by enhanced hardness and resistance to corrosion and wear, whereas the diffusion zone improves the fatigue properties of the nitrided workpiece [7].

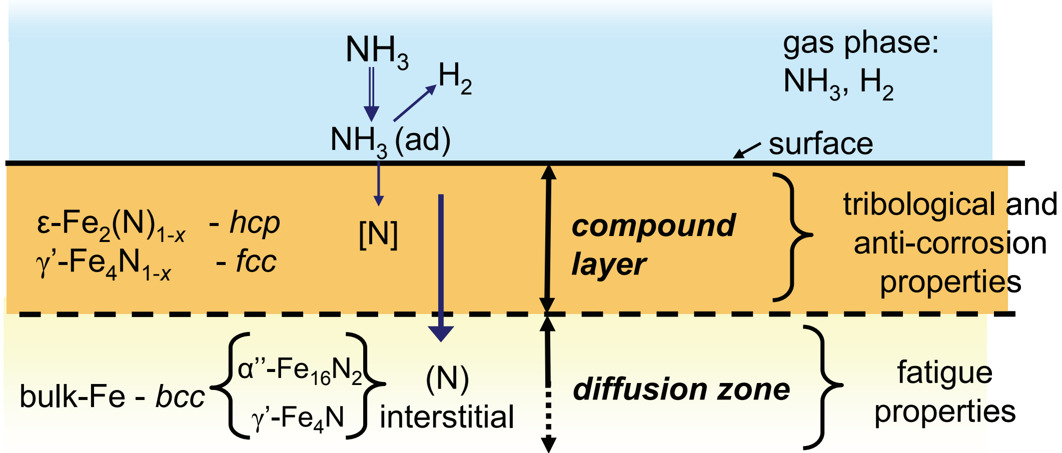

Figure 1.1. Schematic representation of the development of compound layer and diffusion zone as a result of gas nitriding of pure iron. Ammonia provided by an ammonia/hydrogen mixture in the gas phase is adsorbed at the surface of the workpiece and subsequently dissociates into atomic nitrogen ([N]) and hydrogen. By inward diffusion nitrogen reacts with iron forming a compound layer composed of iron nitrides and/or a diffusion zone, where iron nitride precipitates as well as interstitially dissolved nitrogen compose the diffusion zone.

A direct reaction of iron with nitrogen to form iron nitrides is thermodynamically unfavourable at atmospheric pressure. A reaction of iron with ammonia to form iron nitrides, however, produces at 773 K and 10^{-5} Pa a release of Gibbs free energy of about 20 kJ/mol [12]. Thus, in typical gas nitriding processes temperatures between 700 and 860 K and atmospheric pressures are applied to form iron nitrides. The (hypothetical) chemical reactions taking place during the gas nitriding treatment of pure iron can be summarized as follows:

$$1/2\,N_2 \rightleftharpoons [N] \tag{1.1}$$

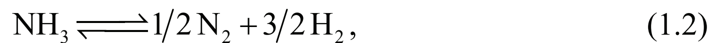

$$NH_3 \rightleftharpoons 1/2\,N_2 + 3/2\,H_2\,, \tag{1.2}$$

resulting in

$$NH_3 \rightleftharpoons [N] + 3/2\,H_2\,, \tag{1.3}$$

where [N] denotes atomic nitrogen dissolved in the ferrite matrix.

Due to the equality of the chemical potentials of nitrogen in the gas and in the solid phase and as a consequence of thermodynamic equilibrium it follows for the nitrogen activity, a_N, in the solid at the solid/gas interface:

$$a_{\mathrm{N}} = \left(p^{0}_{\mathrm{N_2}}\right)^{-1/2} K \left(\frac{p_{\mathrm{NH_3}}}{p^{3/2}_{\mathrm{H_2}}} \right), \tag{1.4}$$

where $p^{0}_{\mathrm{N_2}}$ denotes the reference pressure (1 atm) of the (hypothetical) nitrogen gas as present in equations (1.1) and (1.2), K is the equilibrium constant for equation (1.2) and p_i are the partial pressures of the constituents of the nitriding gas atmosphere. This ratio of partial pressures is called the nitriding potential, r_{N}:

$$r_{\mathrm{N}} \equiv \frac{p_{\mathrm{NH_3}}}{p^{3/2}_{\mathrm{H_2}}}. \tag{1.5}$$

From equations (1.4) and (1.5) it is clear that the nitriding potential is directly proportional to the activity (and thus to the chemical potential) of nitrogen in the gas phase. Besides temperature the nitriding potential therefore serves as a crucial parameter controlling the nitriding process. The binary system Fe-N can thus not only be represented by the conventional phase diagram (see Figure 1.3), but by a modified phase diagram, where the phase fields are drawn as function of temperature and nitriding potential, which is known as the Lehrer diagram [14] (see Figure 1.2).

8. Summary

8.1. Introduction

Microstructure and residual stress state are important properties of thin films which have a significant influence on the physical properties. As an example, a nanocrystalline microstructure can have an impact on phase equilibria or on the coefficient of thermal expansion. Residual stresses in thin films can lead to mechanical failure of a system composed of thin film and substrate due to delamination (in case of compressive residual stresses) or cracking (in case of tensile residual stresses) of the film. The aim of this work is to investigate interrelations of the microstructure and the properties of thin films, particularly the residual stress state, utilizing selected examples.

8.2. Unexpected formation of ε-iron nitride by gas nitriding of nanocrystalline α-Fe films

In the second chapter of this thesis the phase formation during gas nitriding of nanocrystalline iron thin films on inert substrates (α-Al_2O_3 wafers) is investigated. Qualitative phase analysis of the produced iron-nitride films revealed that the phase γ'-Fe_4N_{1-x}, which is expected to form according to the generally accepted „Lehrer diagram“ [1,2] under the conditions applied, indeed has formed. However, strikingly, the phase ε-Fe_2N_{1-x}, which was not expected to form under the nitriding parameters applied, has formed additionally for a specimen exhibiting a very low average lateral crystallite size of about 80 nm (the average lateral crystallite size of films forming exclusively γ'-Fe_4N_{1-x} is about 400 nm).

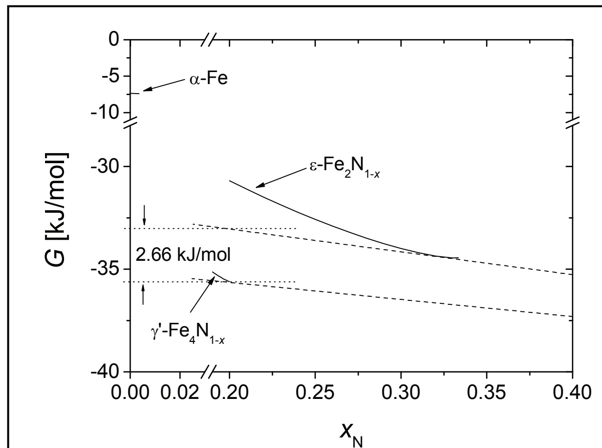

Figure 8.1. Gibbs free energy G as function of the atom fraction nitrogen x_N for α-Fe, γ'-Fe_4N_{1-x} and ε-Fe_2N_{1-x} at $T = 550$ °C, $p = 1$ atm and $r_N = 1$ atm$^{-1/2}$. The double tangents (dashed) to the $G(x_N)$ curves of γ' and ε intersect at $x_N = 1$, which correponds to the chemical potential of nitrogen in the gas phase.

This observation leads to the assumption that a nanoscale grain size may be the reason for the formation of ε iron nitride. The calculation of Gibbs energies, G, of the phases α, ε and γ' as functions of atom fraction nitrogen, x_N, making use of thermodynamic data from Refs. [3-6] (see Figure 8.1) shows that an increase of 2.66 kJ/mol of the Gibbs energy of γ' is necessary, so that the ε phase is stable. This increase can be caused by the Gibbs-Thomson-Effect: $\Delta G = (2\gamma V_m)/r$, where γ is the interfacial energy, V_m the molar volume and r the radius of a nanocrystalline particle of a certain phase [7]. For the radius of the γ' crystallites, which form during nitriding a value of 40 nm can be estimated (cf. chapter 2). It follows that the interfacial energy of the phase γ' is about 1.6 J/m^2, which indeed represents a realistic value [7]. It could thus be shown that the thermodynamics of the system iron-nitrogen can be significantly influenced by a nanoscale crystallite size.

8.3. Crystallite-size dependence of the coefficient of thermal expansion of metals

In literature several contradictory findings concerning a possible crystallite-size dependence of the coefficient of thermal expansion (CTE) were obtained [8-10]. The crystallite-size dependence can be monitored by temperature-dependent in-situ X-ray diffraction (XRD) measurements making use of actual methodological developments.

In the experiments performed in this study Cu and Ni thin films (nominal thickness 50 nm each) deposited onto Si wafers by DC magnetron sputtering at room temperature were employed as specimens. XRD measurements were performed using a diffractometer equipped with a heating/cooling chamber mounted on an Eulerian cradle (cf. chapter 3.2 for details of the XRD measurements).

Firstly, the strain-free lattice parameters of the Cu and Ni films were determined from temperature-dependent in-situ XRD residual stress analysis in the

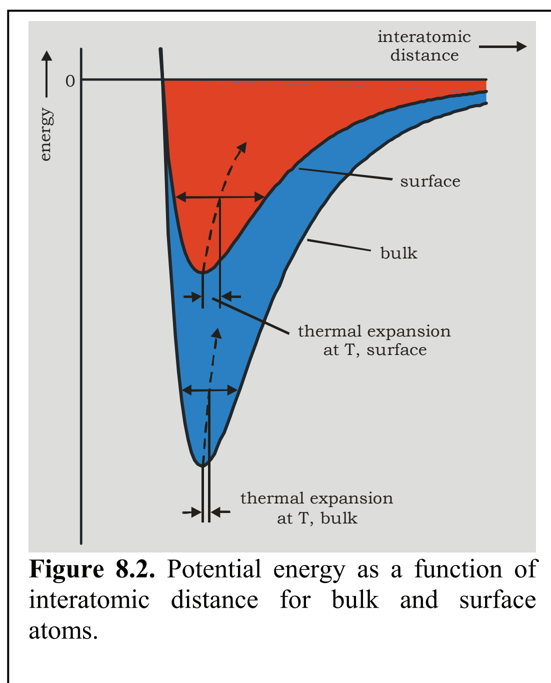

Figure 8.2. Potential energy as a function of interatomic distance for bulk and surface atoms.

range between -100 °C and 25 °C. The CTEs were determined from the slopes of plots of thermal strain, ε_{th} (= $\Delta d/d_0$, where d_0 is the lattice plane spacing at room temperature and Δd is the change of lattice spacing due to a change of temperature ΔT), versus temperature, T. It has been found that the CTEs of the as-deposited nanocrystalline Cu and Ni films were significantly larger than the CTEs obtained for the corresponding coarse-grained bulk materials. It has turned out that it is very important to perform the CTE measurements at temperatures below room temperature, because at temperatures above room temperature the nanocrystalline microstructure coarsens very quickly as could be shown by in-situ XRD measurements. After this coarsening has taken place, the CTEs of the corresponding bulk material are obtained. (Table 7.1).

The dependency of the CTE on crystallite size can be understood considering the states of bonding at grain boundaries and surfaces. Atoms at the surface of a crystal or at an (incoherent) interface (grain boundary) are not saturated with respect to their state of bonding: their coordination number is less than for bulk atoms. As a consequence different potential curves (potential energy versus interatomic distance; see Figure 8.2) follow. For surface/interface atoms the potential curve shows a less deep minimum well and exhibits a larger asymmetry than for bulk atoms. Due to this

Table 8.1. The measured CTE values of the Ni and Cu thin films and the corresponding literature values [11,12]. TF: Thin film specimen, CG: Coarse-grained specimen.

	CTE of Ni [10^{-6}/°C]	CTE of Cu [10^{-6}/°C]
As-deposited (TF)	13.7 ± 0.4	18.8 ± 0.4
After heat treatment (TF)	12.6 ± 0.2	17.4 ± 0.4
Literature value (CG)	12.4	15.7

	Crystallite size *D* of Ni [nm]	Crystallite size *D* of Cu [nm]
As-deposited (TF)	37	26
After heat treatment (TF)	59	41

asymmetry the same thermal energy leads to different thermal expansion for surface/interface and bulk atoms. The smaller a crystallite, the larger the ratio of the number of surface/interface atoms and the number of bulk atoms. Thus, the smaller a crystal, the larger its *average* CTE.

8.4. Determination of gradients of effective grain interaction and stress in Cu thin films

The investigation of the depth dependence of effective grain interaction and residual stresses in Cu thin films by XRD is subject of the fourth chapter of the thesis. In order to create a residual stress gradient the deposition parameters were changed during thin film production. The gradients were analysed by XRD measurements at constant penetration depth (for further details about this method and the corresponding limitations see chapter 4.2.1 and Ref. [13]). Thus, for each penetration depth several diffraction lines *hkl* were recorded over the corresponding accessible ψ range. The absorption of the investigated material was adjusted by variation of the X-ray energy, E, such that a maximum range of penetration depth could be covered. Therefore measurements were performed at a laboratory diffractometer (E = 8.048 kV) and at a synchrotron beamline („Surface Diffraction Beamline“, Ångströmquelle Karlsruhe (ANKA), E = 9.996 kV) (for details of the measurements see chapter 4.3.4). Upon employing small incidence or exit angles (< 2,5°) the effect of refraction has to be considered: For an ideally flat surface this effect leads to a change of incidence or exit beam angles and thus to a change of measured diffraction angle. It is thus necessary to correct the measured diffraction angles employing a refraction correction (for details see Ref. [14] and chapter 4.2.2). If the specimen exhibits a certain surface roughness the effect of refraction is reduced, which leads to an overestimation of the refraction-induced error of the measured diffraction angle (see Ref. [15] and chapter 4.2.2).

The evaluation of the measured lattice spacings was performed on the basis of the $f(\psi, hkl)$ method (see Refs. [16-18] and chapter 4.2.3). Adopting this method it is possible to introduce a weighting parameter, w, which defines effective X-ray elastic constants (XECs) according to $S_{1,2}^{hkl} = wS_{1,2}^{hkl,\mathrm{V}} + (1-w)\,S_{1,2}^{hkl,\mathrm{R}}$, where the superscripts „V“ and „R“ denote the Voigt and Reuss models of elastic grain interaction, respectively. Thus, effective XECs can be determined as function of penetration/information depth by least-squares fitting with w as fit parameter (for further details see chapter 4.2.3).